Lateral Diffusion and Percolation in Two-Phase, Two-Component Lipid Bilayers. Topology of the Solid-Phase Domains In-Plane and Across the Lipid Bilayer†

Paulo F. F. Almeida,‡ Winchil L. C. Vaz,§,‖ and T. E. Thompson*,‡

Department of Biochemistry, University of Virginia, Charlottesville Virginia 22908, and Max-Planck-Institut für biophysikalische Chemie, Postfach 2841, DW-3400 Göttingen, FRG

Received December 9, 1991; Revised Manuscript Received May 14, 1992

ABSTRACT: Fluorescence recovery after photobleaching (FRAP) has recently been used to examine the percolation properties of coexisting phases in two-component, two-phase phosphatidylcholine bilayers [Vaz, W. L. C., Melo, E. C. C., & Thompson, T. E. (1989) *Biophys. J. 56*, 869–876]. We now report the use of FRAP to study two additional problems in similar systems. The first is the effect of solid-phase obstacles on the lateral diffusion in the fluid phase. The second is the question of whether or not, in a single bilayer, solid-phase domains in one monolayer are exactly superimposed on solid domains in the apposing monolayer. To address the first problem, the lateral diffusion of *N*-(7-nitrobenzoxa-2,3-diazol-4-yl)-1-palmitoyl-2-oleoylphosphatidylethanolamine (NBD-POPE), a probe soluble only in the fluid phase when solid and fluid phases coexist, has been studied in the mixture *N*-lignoceroyldihydrogalactosylceramide (LigGalCer)/dipalmitoylphosphatidylcholine (DPPC). Percolation of the fluid phase occurs at a high mass fraction of solid phase. This indicates that the solid domains have a centrosymmetric shape, a characteristic which makes this a good experimental system to test theoretical simulations of diffusion in an archipelago. It is shown that agreement between theory and experiment is poor, a result that had already been observed when the obstacles were integral membrane proteins. We develop an effective-medium model for diffusion in two-phase systems which explains both our results and those obtained with integral proteins. The distinctive feature of the model is the consideration of an annular region around the obstacles where the lipids are more ordered than in the bulk fluid phase. The diffusion coefficient is then calculated by extending the free area model to two-phase systems, taking these annuli into account. The second question, the organization of the solid-phase domains across the lipid bilayer, is examined in the systems LigGalCer/DPPC and dimyristoylphosphatidylcholine (DMPC)/distearoylphosphatidylcholine (DSPC) by comparing the diffusion of a fluid-phase-soluble, gel-phase-insoluble lipid derivative which spans the two monolayers of a bilayer (NBD-membrane-spanning-phosphatidylethanolamine, NBD-msPE) with that of a probe which is restricted to a single monolayer. In LigGalCer/DPPC, 20:80, the distribution of solid domains in one of the monolayers is independent of the distribution in the apposing monolayer. In contrast, in DMPC/DSPC, 50:50, the solid domains in one monolayer are exactly superimposed upon the solid domains existing in the apposing monolayer.

Phospholipid bilayers composed of two or more lipid species have been shown to exhibit phase separations into a solid or gel phase and a liquid-crystalline or fluid phase, in a wide range of temperatures, at constant pressure (Shimshick & McConnell, 1973; Wu & McConnell, 1975; Mabrey & Sturtevant, 1976). An important question concerning the structure of the bilayer is the topology of the phases in equilibrium. One aspect of this problem is the lateral organization of the domains of the two phases and their connectivity properties. If a lipid binary mixture, originally in the fluid state, is cooled down into the coexistence region, solid phase will be formed. As the temperature is further decreased, the fraction of solid increases. Eventually, a point is reached where the solid phase forms a continuous cluster in the plane of the lipid bilayer, thereby disconnecting the previously continuous coexisting fluid phase into isolated domains. This is the percolation threshold of the bilayer (Stauffer, 1985; Saxton, 1982, 1987). At temperatures below this point, for molecules soluble only in the fluid phase, translational diffusion in the whole plane of the bilayer is no longer possible. The solid-phase clusters act as barriers for the diffusion of fluid-soluble particles, and once these clusters make the fluid phase discontinuous, diffusion is possibly only within the limited regions of this phase that have become isolated from each other. It has recently been shown that the technique of fluorescence recovery after photobleaching (FRAP)[1] can be used to detect the point of percolation in phospholipid mixtures (Vaz et al., 1989, 1990; Bultmann et al., 1991). In this work, we have employed the same method to examine the binary mixture of *N*-lignoceroyldihydrogalactosylceramide (LigGalCer) and dipalmitoylphosphatidylcholine (DPPC) using the fluorescent lipid probe *N*-(7-nitrobenzoxa-2,3-diazol-4-yl)1-palmitoyl-2-oleoylphosphatidylethanolamine (NBD-POPE). We have observed that this mixture exhibits a large temperature interval of solid/fluid coexistence where the fluid phase is continuous. When the point of percolation occurs at high mass fractions of solid,

† This work was supported in part by Grants GM-14628 and GM-23573 from the National Institutes of Health and in part by the Max-Planck-Institut für biophysikalische Chemie.

‡ University of Virginia.

§ Max-Planck-Institut für biophysikalische Chemie.

‖ Present address: Unidade de Ciências Exactas e Humanas, Universidade do Algarve, Campus de Gambelas, P-8000 Faro, Portugal.

[1] Abbreviations: DMPC, dimyristoylphosphatidylcholine; DPPC, dipalmitoylphosphatidylcholine; DSPC, distearoylphosphatidylcholine; LigGalCer, *N*-lignoceroyldihydrogalactosylceramide; NBD-DLPE, *N*-(7-nitrobenzoxa-2,3-diazol-4-yl)dilauroylphosphatidylethanolamine; NBD-POPE, NBD-1-palmitoyl-2-oleoylphosphatidylethanolamine; NBD-msPE, NBD-membrane-spanning-phosphatidylethanolamine; FRAP, fluorescent recovery after photobleaching.

0006-2960/92/0431-7198$03.00/0

the solid domains probably have a centrosymmetric shape (Xia & Thorpe, 1988). This feature makes the LigGalCer/DPPC mixture a good test system for evaluating the applicability to lipid bilayers of theoretical treatments of diffusion in an archipelago (Saxton, 1982, 1987, 1989). The results reported in this paper agree only qualitatively with Monte Carlo simulations (Saxton, 1987, 1989). We have therefore developed a theoretical effective-medium treatment which considers the existence of a boundary layer around each solid domain where diffusion of fluid lipid particles is slower than in the bulk fluid phase. This model not only explains our results but also accounts for the discrepancy between theory and experiment in the magnitude of the reduction of the apparent diffusion constant observed in the presence of integral membrane proteins (Saxton, 1987; Blackwell & Whitmarsh, 1990).

Another important topological problem concerns the organization of the solid domains across the lipid bilayer. The question is whether or not solid domains in one of the monolayers of a bilayer are necessarily exactly superimposed upon solid domains in the apposing monolayer. The FRAP technique provides a unique method for investigating this problem. We make use of the fluorescent lipid probe NBD-membrane-spanning-phosphatidylethanolamine (NBD-msPE), which has two NBD-derivatized glyceroethanolamine head groups linked by two complex alkyl chains via two ether bonds on each side (Vaz et al., 1985a). In the LigGalCer/DPPC mixture, we compared the diffusion of this molecule with the diffusion of NBD-POPE. The analysis is conceptually very simple: if the solid-phase domains are necessarily superimposed upon each other in the two monolayers of a bilayer, the diffusional paths of the two probes will be identical; if no superposition exists, the transmembrane lipid will sense more domains in its path and its diffusion will therefore be more restricted. We have also examined this question in a 50:50 mixture of dimyristoylphosphatidylcholine (DMPC) and distearoylphosphatidylcholine (DSPC) by extending a previous study which had used the lipid derivative NBD-dilauroylphosphatidylethanolamine (NBD-DLPE) as a probe (Vaz et al., 1989).

MATERIALS AND METHODS

DMPC, DPPC, and DSPC were purchased from Avanti Polar Lipids, Inc. (Alabaster, AL). LigGalCer was obtained from Sigma Chemical Co. (St. Louis, MO). The purity of the lipids was confirmed by thin-layer chromatography. All lipids were used without further purification. Chloroform solutions of the lipids were prepared and stored at −20 °C. NBD-POPE and NBD-msPE were prepared as described before (Vaz & Hallmann, 1983; Vaz et al., 1985a).

Calorimetry. Multibilayer vesicles in excess water were prepared by mixing the two components together in chloroform solution and evaporating the solvent in a rotary evaporator at 60 °C. The samples were then dissolved in toluene/ethanol, 5:1, lyophilized, and redissolved in chloroform. After at least 30 min, the evaporation step was repeated and the samples were placed under high vacuum for 4 h, at room temperature. Hydration of the samples was done at 100 °C with 10 mM HEPES buffer, pH 7.6 (at 20 °C), 50 mM KCl, 1 mM EDTA, 0.02% NaN_3. The dispersions were then stirred for a short period at 90–95 °C, rapidly cooled to 60 °C (70 °C in the case of the 50:50 mixture) and then cooled at less than 5 °C/h to room temperature, and incubated for about 24 h.

The heat capacity curves were determined using a differential scanning calorimeter (Suurkuusk et al., 1976) which was modified to allow scanning at a constant rate. The scan rate used was 10 °C/h, in the heating mode. Preliminary scans were started at 25 °C and ended at 90 °C to ensure that there would be no unnoticed ceramide-rich fraction melting at a high temperature. The final scans were terminated about 10 °C above the completion of the transition.

Lipid concentrations in the hydrated samples were determined by phosphate assay (Bartlett, 1959).

FRAP Experiments. Multibilayers were prepared as previously described (Vaz et al., 1989), with minor modifications. Aliquots (2–3 mg) of lipid were mixed with the NBD probe (at a probe to lipid molar ratio of 1:1000 or 1:2000 for NBD-POPE and NBD-msPE, respectively) in chloroform solution and allowed to stand for 30 min at about 40 °C because of the lower solubility of the ceramide in chloroform. The solvent was then evaporated to a volume of about 0.1 mL and the solution deposited on a siliconized microscope slide at 80 °C, making a lipid film deposit of about 1 cm^2. The microscope slide was placed in a vacuum desiccator over anhydrous calcium chloride granules for 4 h and then warmed to 90 °C in an oven for 10 min. Hydration was performed at this temperature by depositing a 75-μL drop of 10 mM phosphate buffer, pH 7.5, containing 50 mM KCl, 0.02% NaN_3, on the microscope slide and forcing it to spread over the lipid film with the aid of a cover slip. The samples, now in excess water, were then incubated for 2 h at a temperature above which the lipid mixture is completely in the liquid-crystalline state and finally cooled slowly to room temperature over about 4 h. The edge of the cover slip was sealed with a silicone paste (Bayer AG, Leverkusen, FRG) to prevent water evaporation. Samples were left in the dark for 2–15 days before measurements. The multibilayers used for FRAP experiments were selected by inspection with polarization microscopy. The FRAP measurements were made using a circular beam profile with a radius of 3 μm, with the 488-nm line of an argon ion laser. The laser output of 200 mW was split into a monitoring a bleaching beam with an intensity ratio of 10^{-4}. A Zeiss Neofluar 10/0.3 objective was used in these experiments. The temperature of the sample was controlled by a Peltier temperature control unit (Cambridge Thermionic Corp., Cambridge, MA) built into the microscope stage; the temperature control is accurate to about ±0.15 °C. Further details of the apparatus can be found in a previous publication (Vaz et al., 1989). The measurements were begun at a temperature above the liquidus line in the phase diagram for the composition examined. The samples were cooled by changing the temperature in the control unit by 1–2 °C and waiting for a period of at least 30 min at that final temperature before each measurement. After 2 days, the measurements were repeated on the same sample in the heating mode under the same conditions. The bleaching times were of the order of 30–60 ms. The fluorescence recovery was monitored for a period of 30 s to 2 min as appropriate, and the data were collected in a total of 1000 channels. Care was taken to avoid bleaching by the monitoring beam by measuring the fluorescence intensity for a period of time equivalent to the one of an actual experiment, but without the bleaching pulse. The recovery curves were fitted to the theoretical equations (Soumpasis, 1983) using the Simplex algorithm (Quantum Chemistry Exchange Program, Chandler, J. P., Oklahoma State University, Stillwater, OK). When there were more than one diffusing component, the slow components were approximated by a linear ramp as described elsewhere (Vaz et al., 1989).

Theory. On the basis of free-volume theory for diffusion in liquids and glasses (Cohen & Turnbull, 1959) and its

extension to a free-area theory for diffusion of lipids in bilayers, modeled as pseudo-two-dimensional systems (Vaz et al., 1985b; Clegg & Vaz, 1985), we have derived an expression for the diffusion coefficient in the region of solid/fluid coexistence of a two-component lipid mixture (see Appendix). In our model, solid domains are composed of units which are obstacles for the diffusion of fluid-phase-soluble lipid particles. The units, or obstacles, are assumed to be disks of uniform radius. They also affect the fluid-phase lipids in their neighborhood by increasing their orientational order, in a manner similar to the proposed effect of proteins on adjacent lipids (Marčelja, 1976; Owicki et al., 1978; Owicki & McConnell, 1979; Jähnig, 1981) [for a review and further references, see Abney and Owicki (1985)]. We obtained the following expression for the relative diffusion coefficient of a lipid in the neighborhood of a solid domain obstacle:

$$D^*(r) = \frac{D}{D_0} = \exp\left[\left(\frac{a_s}{a_{f_0}}\right)\left(1 - \frac{1}{u(r)}\right)\right] \qquad (1)$$

where D_0 is the diffusion coefficient in the unperturbed bulk fluid phase; the relative free area, $u(r) = a_f/a_{f_0}$, where a_f is the free area per molecule and a_{f_0} is the free area per molecule in the bulk fluid phase; and a_s is the area per lipid in the solid phase. Note that $u = 0$ in the solid and $u = 1$ in the fluid. In the neighborhood of the obstacles, u changes as an exponential decay function with a coherence length ξ (see eq A1 and Figure 9); ξ should have a value of about 15 Å (Jähnig, 1981).

When solid and fluid phases are present, the relative diffusion coefficient $\langle D \rangle$ (see Appendix for definition) becomes an average of $D^*(r)$ over the different regions that compose the entire system: solid disks, annular regions, and bulk fluid. The expression for $\langle D \rangle$ is given by eq A11 (Appendix). In the analysis of the LigGalCer/DPPC mixture, we have assumed the radius of the obstacles to be constant. We fit the diffusion data to eq A12, which is the numerical form of eq A11. Allowing for a variable radius as a function of temperature resulted in no improvement of the fit. The coherence length ξ of the obstacle-induced perturbation was kept constant (see Appendix for a discussion of this aspect).

RESULTS

Calorimetry and Area Fractions of Solid and Fluid Phases. In order to evaluate the amounts and areas of solid and liquid phases coexisting at a given temperature in the LigGalCer/DPPC system, we have recorded the curves of the heat capacity as a function of temperature. These curves are shown in Figure 1A, for mole fractions of ceramide of 0.10, 0.20, 0.33, and 0.50. A partial phase diagram was generated and is shown in Figure 1B. The onset and completion temperatures were determined by arbitrarily leaving out 5% of the total heat, at each side. The reason for this option is the fact that some of the curves have extremely long tails which renders the solidus and liquidus lines impossible to determine without some assumption regarding the onset and completion temperatures of the transitions. The methods most often used consist of extrapolating the heat capacity curves from some region close to the baseline, which is also arbitrary, and correcting for the finite width of the transition, which has no meaning in cases where the transition obviously occurs over a wide range of temperatures (Maggio et al., 1985a). The particular choice of onset and completion temperatures does not affect our results because the mass fractions of solid and fluid phases coexisting at each temperature were calculated by direct integration of the heat capacity function. This is possible in the case of the

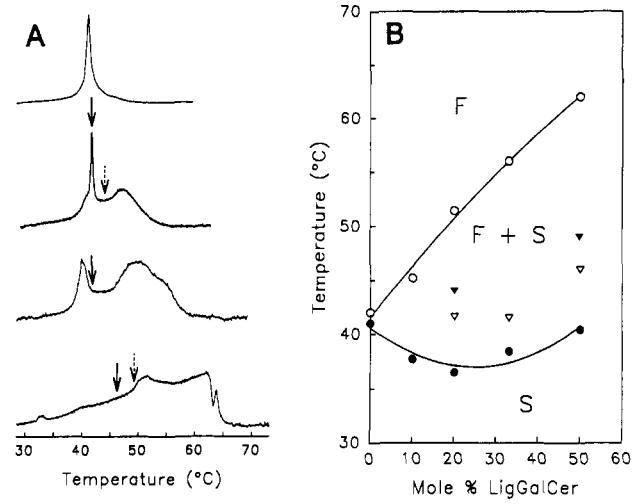

FIGURE 1: (A) Calorimetric scans of several compositions of the binary mixture LigGalCer/DPPC: mole ratios (from top to bottom) 10:90, 20:80, 33:67, and 50:50. (B) Partial phase diagram of the same mixture: F, fluid phase; S, solid phase. The onset (●) and completion (○) temperatures of the transition are indicated. The curves are smooth lines drawn through the points. The apparent percolation points determined with NBD-POPE and NBD-msPE (see text) are indicated in (A) by the solid and dashed arrows, respectively, and in (B) by ▽ and ▼.

LigGalCer/DPPC mixture because the enthalpy of the main transition is very similar for both lipids: 8.7 kcal/mol for DPPC (Mabrey & Sturtevant, 1976) and 7.3 kcal/mol for LigGalCer (Maggio et al., 1985b). We have estimated the bias affecting the calculated mass fractions of solid and fluid phases by decomposing the heat capacity curve into several transitions each corresponding to a given composition (the enthalpy being a weighted average of the enthalpies according to the composition). The effect is extremely small, the two methods giving results that are indistinguishable within the experimental uncertainty. No transitions were observed above 70 °C in any of the samples examined. All values of the total enthalpy of the transition fall in the range of 8.7 ± 0.9 kcal/mol. No consistent trend with change in composition was detectable for the mixtures examined (LigGalCer/DPPC 10:90, 20:80, 33:67, and 50:50). This further supports the validity of using direct integration to evaluate the masses of phases in equilibrium. The fractional areas of each phase were calculated by using a value of 45 Å^2 for the area of a solid-phase lipid molecule (Wiener et al., 1989) and 63 Å^2 for a fluid-phase molecule, regardless of the composition of the phases. These area assumptions are not rigorous, but there is no information available for the areas per molecule in two-component phases. These values are accurate to about ±2 Å^2 for DPPC. They can be calculated from a knowledge of the thickness and the volume of the lipid bilayer. [See, for sources of pertinent information, Wilkinson and Nagle (1978), Lewis and Engelman (1983), Sankaram and Thompson (1990), and Almeida et al. (1992)]. The temperature dependence of the molecular areas in a given phase is weak and was not taken into account in our calculations.

FRAP Experiments. Both NBD-POPE and NBD-msPE partition essentially exclusively into the fluid phase when solid and fluid phases coexist in a lipid bilayer, as estimated by fluorescence polarization spectroscopy (W. L. C Vaz, unpublished observations), and also in monolayers (R. Tillmann, H. E. Gaub, and W. L. C. Vaz, manuscript in preparation). We use NBD-POPE in the LigGalCer/DPPC mixture instead of the previously employed NBD-DLPE because we are dealing here with relatively long-chain lipids, and their

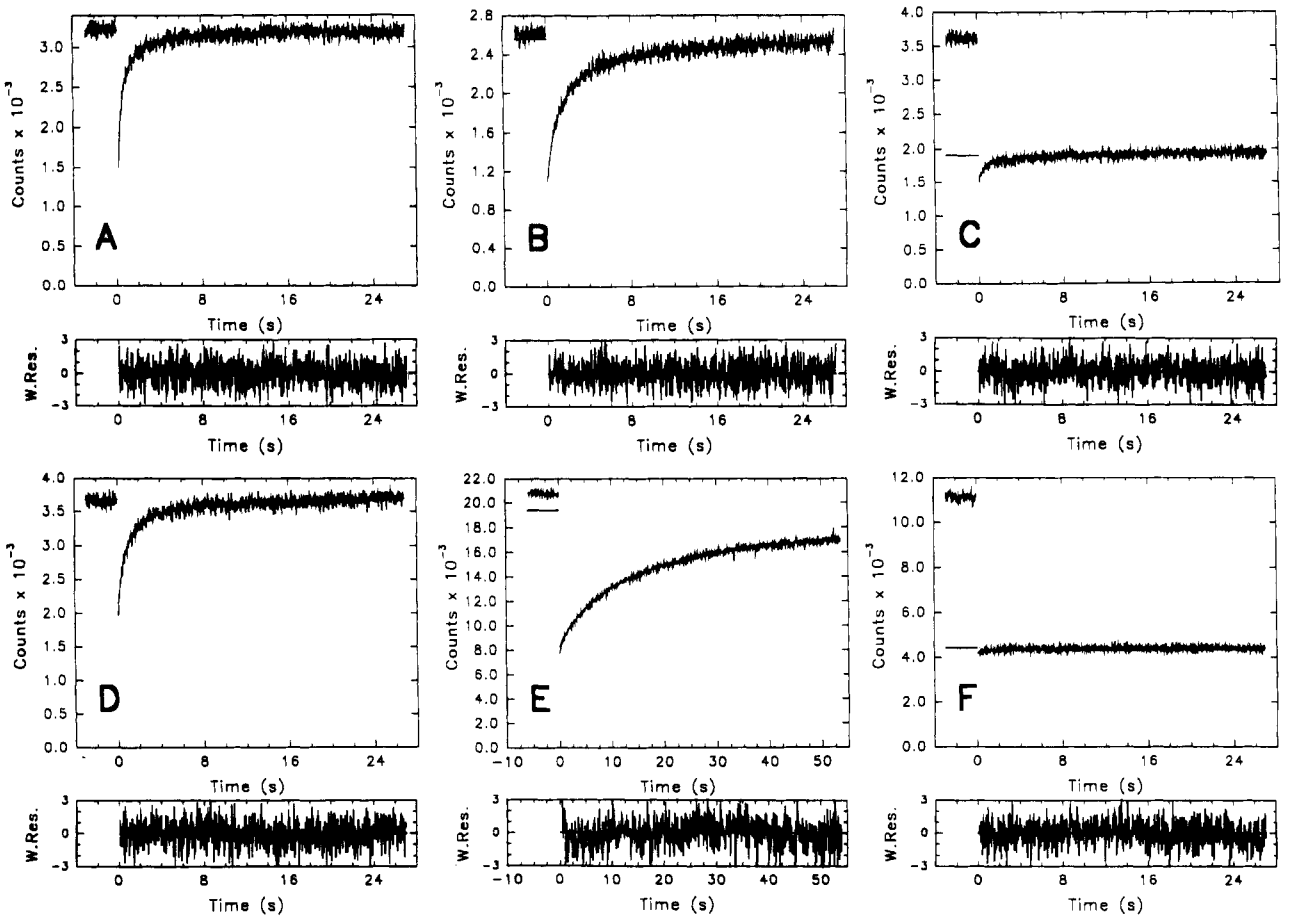

FIGURE 2: Typical recovery curves in a FRAP experiment in LigGalCer/DPPC, 20:80. A–C were obtained in one cooling scan with NBD-POPE; D–F were obtained in one cooling scan with NBD-msPE. The temperatures and fit parameters are as follows: (A) 56.0 °C, τ = 0.268 s, slope = 0.0 counts/s, recovery 99.5%, χ^2 = 1.1; (B) 44.0 °C, τ = 1.060 s, slope 0.7 counts/s, recovery 97.0%, χ^2 = 1.1; (C) 38.0 °C, τ = 0.445 s, slope 2.7 counts/s, recovery 22.0%, χ^2 = 1.0; (D) 56.0 °C, τ = 0.474 s, slope 1.4 counts/s, recovery 100.6%, χ^2 = 1.2; (E) 44.0 °C, τ = 12.1 s, slope 0.0 counts/s, recovery 89.8%, χ^2 = 1.7; (F) 40.0 °C, σ = 0.752 s, slope counts/s, recovery 4.2%, χ^2 = 1.1. The values of τ indicated are not corrected by the exact radius of the laser spot in each individual experiment; normalization to a 3-μm spot would lower each value by about 10% in these two particular cooling experiments. The horizontal lines on the left side of each panel indicate the limiting value of the recovery (time $\rightarrow \infty$). The bottom panels show the weighted residuals in units of standard deviations.

interactions with a short-chain probe may be poor even in the fluid phase, possibly leading to phase separation of the probe or desorption from the bilayer.

Figure 2 shows some typical fluorescence recovery curves recorded on multibilayers formed from LigGalCer/DPPC, 20:80, at three different temperatures, for both probes, NBD-POPE and NBD-msPE. When the system is entirely in the fluid phase, a rapid and complete recovery is observed (Figure 2A, D). At 44 °C, in the mixed-phase region, diffusion is considerably hindered as shown by the slower recovery time (Figure 2B, E), the effect being more pronounced with NBD-msPE than with NBD-POPE in the fluid phase, in this system. It is apparent that the fit is not perfect in the beginning of the curve in Figure 2E. This probably reflects the existence of a small fraction of fast-recovering components corresponding to diffusion in small fluid areas that have already become isolated from the main fluid phase by solid-phase clusters. Below 41.5 °C, a very limited recovery is observed in the case of NBD-POPE (10–25%) and almost no recovery occurs with NBD-msPE (Figure 2C, F, respectively); the recovery time of this small fraction, however, is relatively fast, though impossible to determine with certainty in the case of NBD-msPE.

Percolation and Variation of the Recovery Time (τ) with Temperature: Diffusion of NBD-POPE. When a sample of multibilayers is cooled from a temperature at which the whole system is in the fluid state down into the mixed-phase region, two important changes occur. First, the recovery ceases to be 100%, and second, τ increases more rapidly as the temperature is decreased. This is shown in Figure 3 for diffusion of NBD-POPE in LigGalCer/DPPC, 20:80, where the points corresponding to two cooling and two heating curves are represented. The process has virtually no hysteresis, which strongly suggests that the system is at equilibrium at each point in temperature. It is apparent, moreover, that a unique point exists where the precent recovery precipitously drops from almost 100 to about 15% *and* the recovery time τ increases abruptly, reaching a maximum at about 41.5 °C. We interpret this point as identifying the percolation threshold (Stauffer, 1985; Saxton, 1982, 1987) in the plane of the lipid bilayer and shall refer to it as such in this paper. The problems involved in this interpretation will be further developed in the Discussion. The points of percolation were also determined in LigGalCer/DPPC, 33:67 and 50:50; they are indicated in Figure 1 on the heat capacity curves (A) and on the phase diagram (B). The percolation thresholds occur at very high area fractions of solid phase, in all case: 0.71, 0.74, and 0.75, for the 20:80, 33:67, and 50:50 mixtures.

Domain Organization across the Lipid Bilayer: Diffusion of NBD-msPE. In the two mixtures examined in this work, LigGalCer/DPPC and DMPC/DSPC, the lipid probe NBD-msPE diffuses slower than NBD-POPE and NBD-DLPE by

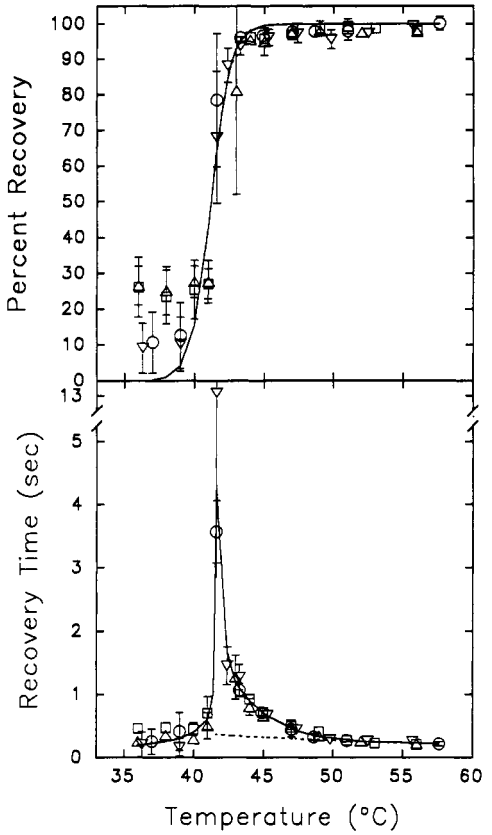

FIGURE 3: Percent recovery and recovery time as a function of temperature in LigGalCer/DPPC, 20:80, measured with NBD-POPE: ○, □, cooling scans in two different samples; △, ▽, heating scans in two different samples. The points represent averages of four measurements, and the error bars are the corresponding standard deviations. For the lowest four points in the upper panel and the corresponding points in the lower panel, fewer measurements were made; for this reason, for some of these points the standard deviations were estimated on the basis of other observations in the same region of the plot. The dashed line in the recovery time plots represents the behavior expected for a hypothetical system with the same composition, but where no solid formation would occur (reference state, τ_0). It was obtained by extrapolation of the behavior of τ in the fluid state. Its slope results simply from the temperature dependence of the diffusion coefficient in the fluid phase. The apparent activation energy of 7.0 kcal/mol is very close to the 6.5 kcal/mol calculated for pure DPPC from the data of Vaz et al. (1985b). For temperatures higher than that of the percolation threshold, the solid line was calculated from the fit to eqs A11/A12 and the baseline (τ_0); below this temperature it is a line drawn through the points.

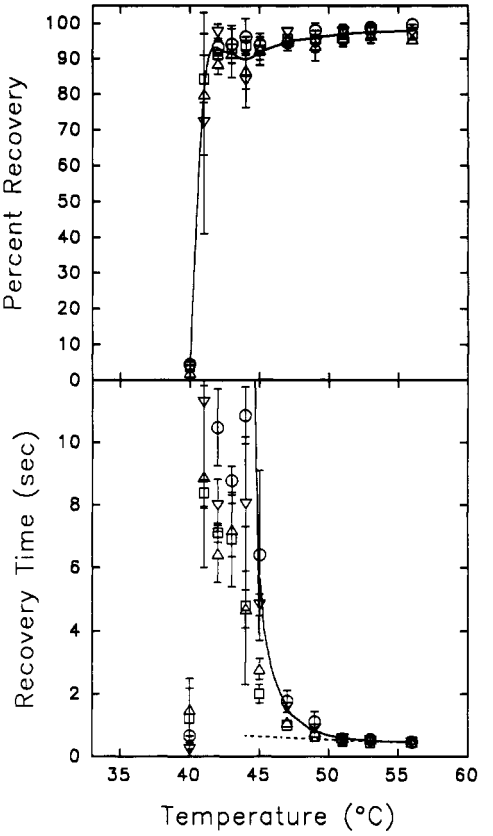

FIGURE 4: Percent recovery and recovery time as a function of temperature in LigGalCer/DPPC, 20:80, measured with NBD-msPE. Symbols and lines are as in Figure 3. Notice that the scale in the recovery time plot differs from that in Figure 3 by a factor of 2, corresponding to a factor of 2 in the relation between the diffusion coefficients of the two probes in the fluid phase, in this mixture. Four different points are essentially overlapping at the three highest temperatures. In the calculation of the solid line, the solid fraction used is the effective solid area fraction sensed by the transmembrane probe (see Discussion).

a factor of 2 when the systems are completely in the fluid state. Figure 4 shows the variation of τ and the percent recovery as a function of temperature in the mixture LigGalCer/DPPC, 20:80. When compared to the diffusion of NBD-POPE (Figure 3), it is apparent that a qualitative difference exists: the value of τ rises abruptly at approximately 44 °C instead of at 41.5 °C. This abrupt increase in τ identifies the apparent percolation point of the system as sensed by NBD-msPE. It occurs at a solid area fraction of 0.45 and 0.65 in the 20:80 and 50:50 mixtures of LigGalCer/DPPC, respectively. The percent recovery does not show a major change before 41.5 °C. However, below 44 °C, the fits are not very good and the value of τ obtained may represent another process or combination of processes and not only the diffusion of lipid molecules. Another aspect to be considered is that the solid domains are probably smaller at 44 °C than at 41.5 °C, the percolation point determined by NBD-POPE; their mobility is therefore expected to be higher. The obstacles must be immobile in the time scale of the measurement for percolation to be observed (Saxton, 1987). Nevertheless, the percent recovery does show an abnormal behavior at 44 °C, with a slight decrease in its value and an increase in the dispersion.

We have also examined the behavior of the probe NBD-msPE in the binary lipid mixture DMPC/DSPC with a 50:50 molar composition. This system had previously been studied with NBD-DLPE (Vaz et al., 1989). Figure 5 shows the cooling and heating scans for the dependence of the percent recovery on temperature for each probe. Two aspects are evident: the cooling curves are essentially the same for the two probes whereas the heating curves are different, and there is considerable hysteresis in the experiment with NBD-msPE, but not with NBD-DLPE. The values of τ obtained with each probe coincide in the solid/fluid coexistence region in the cooling scan (data not shown), except for a factor of 2 corresponding to the intrinsic difference in diffusion of the two probes. With NBD-msPE, the values of τ are slightly higher in the heating than in the cooling scan, but the difference is probably not significative (the standard deviation ranges overlap). In order to determine which was the equilibrium curve, we cooled the system in steps of 2 °C and, at 39 °C, followed the change in percent recovery with time. Then the sample was cooled again in steps of 2 °C into the solid phase. After 8 days at 20 °C, the process was repeated in the heating mode and stalled at 39 °C. Again we followed the change in percent recovery with time. No change occurred in the percent recovery when the measurements were performed upon stalling in the cooling mode, but the recovery continuously changed

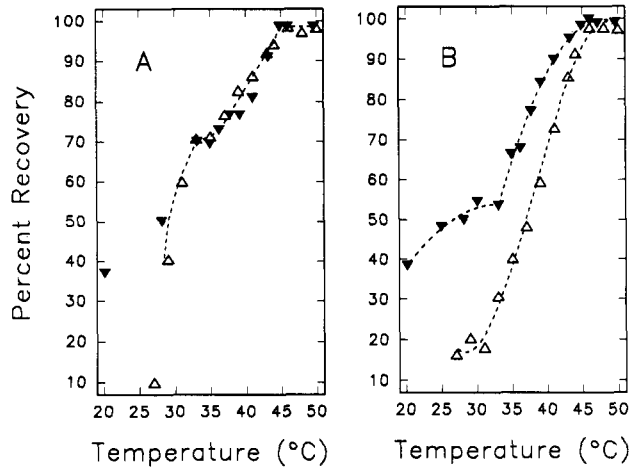

FIGURE 5: Percent recovery as a function of temperature in the mixture DMPC/DSPC, 1:1: (A) Cooling scans; (B) heating scans. Points correspond to experiments using NBD-msPE (△) and NBD-DLPE (▼). Each point is an average of at least eight measurements in two (NBD-msPE) or five (NBD-DLPE) different samples. The curves are smooth lines drawn through the points. Data corresponding to NBD-DLPE are from Vaz et al. (1989).

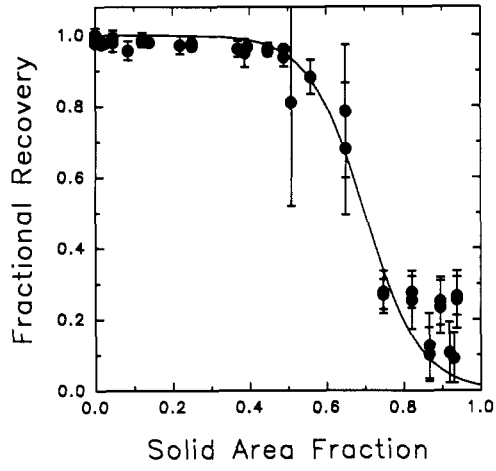

FIGURE 6: Fractional recovery as a function of solid area fraction in LigGalCer/DPPC, 20:80, using the probe NBD-POPE. The data are replotted from Figure 3 using the solid- and liquid-phase areas per molecule given in the text. The points represent averages of four measurements and corresponding to two cooling and two heating scans. Error bars are standard deviations. The curve is a fit to the equation Recovery = $1/\{1 + \exp[k(c - c_p)]\}$, where c_p is the apparent percolation point, c is the solid area fraction, and k is a constant. Whereas this equation may have no theoretical significance, it describes the data quite well and allows for a calculation of the inflection point, $c_p = 0.70$.

with time at 39 °C in the heating scan (data not shown). The equilibration process has an apparent half-time of at least 7 h, if we analyze it as a simple exponential function. We conclude therefore that the curve corresponding to equilibrium is the cooling scan.

DISCUSSION

General Interpretation of the Diffusion of NBD-POPE in LigGalCer/DPPC. The study of diffusion in the LigGalCer/DPPC mixture has revealed the existence of a unique point which is apparent as an inflection in the function describing the change of the percent recovery with the solid fractional area (Figures 3 and 6) and as a maximum in the curve representing τ as a function of temperature (Figure 3). We have identified this point with the percolation threshold of the system (Stauffer, 1985) in the plane of the bilayer. In LigGalCer/DPPC, 20:80, it occurs at a solid area fraction of 0.71. According to continuum percolation theory (Xia and Thorpe, 1988) this probably means that the units constituting the solid phase are nearly circular. Note, however, that the actual solid domains are composed of several of these units and may have an irregular shape. The percolation point predicted for random overlapping disks in a continuum occurs at an area of disks of 0.67 (Xia & Thorpe, 1988). It is important to keep in mind, however, that there is no a priori guarantee that this lipid mixture can be treated as a random quenched system; the lipid domains cannot physically overlap although the shape of irregular domains can in principle be described by the use of overlapping circles. We would therefore prefer to keep the interpretation in a qualitative or a semiquantitative frame. Above the percolation threshold (higher temperatures), as the temperature decreases τ increases because the solid domains formed act as barriers to diffusion in the fluid phase (Saxton, 1982, 1987). In this temperature region a lateral diffusion coefficient (D) can be calculated from $D = \omega^2/4\tau$ (Soumpasis, 1983), where ω is the radius of the bleached spot. Below the percolation point (lower temperatures), τ decreases again because the fluid phase is no longer completely continuous, and diffusion only takes place within small (isolated) fluid domains and not over the whole plane of the bilayer. Within these domains diffusion is fast, as would be expected. The small recovery amplitude occurs because some of these fluid-phase domains are located across the circumference of the bleached spot and are therefore only partially bleached. Below the percolation threshold, the values of τ are not related to the diffusion coefficient in a simple way.

Solid-Phase Domains and Integral Proteins as Obstacles for Lipid Diffusion: Comparison of Theory with Experiment. If the shape of solid domains can be approximated by juxtaposition of nonoverlapping randomly distributed circles, this lipid mixture provides us with an experimental system that can be used to test available models describing diffusion in an archipelago (Saxton, 1982, 1987, 1989). The mixture LigGalCer/DPPC, 20:80, is also attractive because the coexistence region of fluid and solid phases extends over a large temperature interval (about 12 °C), allowing measurements at a number of different solid fractional areas. Saxton (1989) studied the dependence of the diffusion coefficient of a test particle moving in a two-dimensional triangular lattice on the size of hexagonal impenetrable obstacles. His Monte Carlo simulations show that the diffusion coefficient of the test particle decreases with decreasing size of the obstacles, at a constant obstacle area. On the basis of these simulations, it is possible to calculate the average size of the solid domains. In Figure 7 is represented the observed dependence of the diffusion coefficient on the solid area fraction in LigGalCer/DPPC, 20:80. Using the results for immobile obstacles at 0.3 obstacle area fraction [Figure 5 of Saxton (1989)], we determined the size of the hexagons that corresponds to a reduction in the diffusion coefficient identical to that which we observe experimentally. With a solid-phase molecular area of 45 Å^2, this gives 14 solid-phase lipid molecules per obstacle, or 8 Å of radius if the obstacles are modeled as circles with an equal area. If this number were correct, the lifetime of the solid domains would probably be too short in the time frame of the lipid diffusion for the observation of its effects as obstacles on the percent recovery and τ in a FRAP experiment. The mobility of such small domains would also be very high, in the same range as observed for integral membrane proteins formed by a single α-helix (Clegg & Vaz, 1985). These two aspects combined would probably have the effect of abolishing

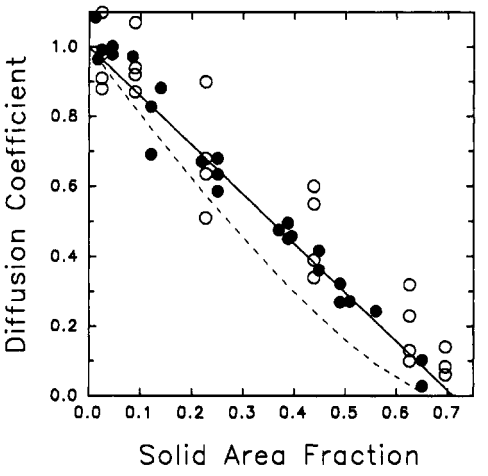

FIGURE 7: Relative diffusion coefficient $\langle D \rangle$ as a function of solid area fraction in LigGalCer/DPPC, 20:80, using the probes NBD-POPE (●) and NBD-msPE (○). This diffusion coefficient is a ratio of the observed value (D) to the hypothetical value which would be observed in the same system if no solid formation would occur (D_o). $\langle D \rangle = \tau_o/\tau \equiv D/D_o$, where τ_o is the baseline in Figures 3 and 4 for NBD-POPE and NBD-msPE, respectively. The solid area fractions corresponding to the points obtained with NBD-msPE are the effective solid areas sensed by this probe, assuming complete randomness for the transbilayer organization of the solid domains (see text). The solid line is the best least-squares fit of eqs A11/A12 to the points corresponding to NBD-POPE and gives $R/\xi = 8.1 \pm 0.4$. The percolation threshold given by the model, i.e., the intercept at $\langle D \rangle = 0$, is $c = 0.71$. The dashed line is calculated using the conductivity eq 28 of Xia and Thorpe (1988) with $t = 1.3$.

the percolation threshold (Harrison & Zwanzig, 1985; Saxton, 1987), whereas our experimental results indicate it exists. Moreover, if the obstacles are mobile, their effect on diffusion of a lipid molecule is smaller (Saxton, 1987). It thus becomes necessary to invoke even smaller obstacles to explain the magnitude of the reduction observed in the diffusion coefficient of a lipid (Saxton, 1989).

The prediction of domains of such a small size probably reflects an underestimation of the effects of obstacles by the Monte Carlo simulations. This problem has already been pointed out by Saxton (1987) and more recently by Blackwell and Whitmarsh (1990), who compared the predictions of three available theoretical models (Pink et al., 1981; Saxton, 1987; O'Leary, 1987) with the measurements of the effect of integral membrane proteins on the diffusion of the lipid particle plastoquinone. All models predict effects that are about 1 order of magnitude smaller than experimentally observed (except when the protein used is gramicidin, where the agreement is good). An explanation sometimes proposed is an increase of the bulk viscosity the lipid bilayer caused by the proteins. This cannot be the sole reason because, within the classical treatment (Einstein, 1926), the increase in the viscosity of a suspension is independent of the size of the particles dispersed in it. This prediction is not in agreement with what we have observed in lipid systems, where the reduction of the diffusion coefficient with increase of solid phase is different in different lipid systems having the same fractions of solid and fluid [compare Vaz et al. (1989), Bultmann et al. (1991), and this study], and with the results obtained with proteins (Blackwell & Whitmarsh, 1990), where a dependence on the protein size is observed. In Einstein's theory, no interactions between the solvent molecules and the suspended particles are considered.

We present here a new theoretical model (Appendix) which accounts for the effects of solid-phase obstacles on the diffusion of lipids (Figures 3 and 7). The solid-domain obstacles are modeled as disks which constitute obstacles for diffusion in the plane of the bilayer as described by Saxton. The fundamental modification we introduce is that a boundary area exists around each obstacle, *extending more than just one lipid layer* into the fluid, where the order of the lipid molecules is increased compared to that in the bulk fluid phase (Figure 9). That this might play an important role in diffusion in lipid bilayers has also been recently suggested by Sperotto and Mouritsen (1991). In the present treatment, this effect is emphasized because of the exponential dependence of the diffusion coefficient on free area, as predicted by free-volume theory. The obstacles are assumed to have a constant radius, and their number is increased as more solid phase is formed. This assumption does not mean, however, that the solid domains do not grow as the temperature is lowered. The disks are to be interpreted as the building blocks of the actual solid domains; the latter will grow with increasing obstacle density. The model is scale-invariant, the only true parameter being the reduced radius R/ξ. Therefore, in the quantitative analysis of our diffusion results, the radius R of the solid-phase obstacles was determined in units of the coherence length ξ. We fit eqs A11/A12 to the experimental data for diffusion of NBD-POPE LigGalCer/DPPC, 20:80, using a nonlinear least-squares analysis. The value $R/\xi = 8.1 \pm 0.4$ was obtained. For example, a value of $\xi = 10$ Å would lead to a radius of 80 Å corresponding to about 400 lipid molecules per obstacle. The actual domains would then contain up to a few thousand molecules. Although an exact calculation of the size of the solid domains is impossible, our results require the existence of solid clusters over the entire range of solid/fluid coexistence and are incompatible with any model which assumes the solid to be essentially one bulk phase. This is the only way of explaining the magnitude of the reduction observed in the diffusion coefficient with increase in solid fraction.

We have used the model to inpret the data on the effect of proteins on the lateral diffusion of lipid particles in bilayers (Blackwell & Whitmarsh, 1990). The agreement with the experimental results is good, as judged by the best fits of eqs A11/A12 to the data (Figure 8). The radii of the proteins were calculated from the cross-sectional area of the proteins (as indicated by the authors), assuming a circular shape. The results of the fits are given in the legend of Figure 8. For the first five proteins (A–E) they lead to $\xi = 22.4 \pm 1.6$ (average ± SD). In striking contrast, for gramicidin (F) $\xi = 1$. These results are not too surprising given the peculiar structure of gramicidin, which has virtually nothing in common with the other integral proteins studied. Gramicidin has a molecular mass of 2 kDa whereas the other proteins range from 33 to 250 kDa (Blackwell & Whitmarsh, 1990). This much smaller mass may decisively hamper the ability of gramicidin to induce order in the adjacent lipids. Accordingly, its obstruction of diffusion is in good agreement with Saxton's (1987) simulations, which take into account only hard core repulsions. Another feature of gramicidin is that it does not have an aqueous domain. It is possible that in the other integral proteins this extramembraneous domain also plays a role in the ordering of adjacent lipids. This would explain why the value of ξ obtained is slightly higher than we had expected. The experiments of Blackwell and Whitmarsh were performed at room temperature so that ξ should be larger than in our experiments, which were carried out at 40–50 °C, but this would only account for about 2-Å difference in ξ (Appendix).

An important question is the effect of obstacle mobility on tracer diffusion. In Monte Carlo simulations (Saxton, 1987, 1988, 1989, 1990), mobile obstacles are less effective in restricting diffusion of a tracer. While the diffusion coefficient

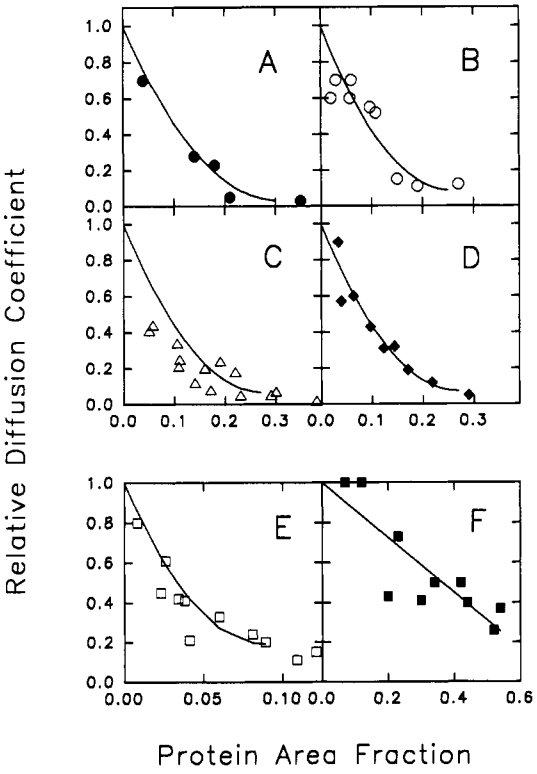

FIGURE 8: Relative diffusion coefficient of the lipid-soluble molecule plastoquinone, as a function of protein area fraction, for four different integral membrane proteins. The reference state is a bilayer without proteins having the same lipid composition. The points were taken from Blackwell and Whitmarsh (1990) and correspond to reaction centers from *Rhodobacter sphaeroides* (A), cytochrome bc_1 from beef heart mitochondria (B), cytochrome *bf* from spinach chloroplasts (C), cytochrome oxidase from beef heart mitochondria (D), cytochrome *f* from spinach chloroplasts (E), and gramicidin D (F). Using the cross-sectional areas given by Blackwell and Whitmarsh and assuming circular cross-sectional shapes, the protein radii were calculated giving (in Å) R = 24.6 (A), 24.0 (B), 21.0 (C), 22.2 (D), 5.35 (E), and 8.0 (F). The lines are best fits of eqs A11/A12 to the data. They correspond to R/ξ = 1.1 (A), 1.0 (B), 1.04 (C), 1.03 (D), 0.221 (E), and 8.5 (F).

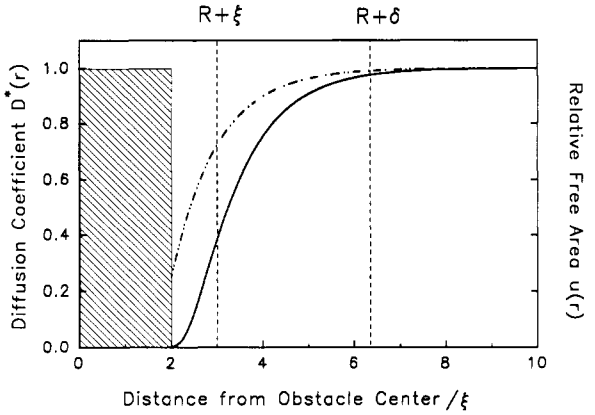

FIGURE 9: Distance dependence of the relative free area $u(r)$ (dashed–dotted curve) and the relative diffusion coefficient $D^*(r)$ (solid curve) away from a solid-phase obstacle (hatched area) in units of ξ. The values are ratios to the corresponding quantities in the bulk fluid phase. ξ is the coherence length of the decay function describing the behavior of the free area. δ is the length within which the influence of the obstacle is appreciably felt. See eqs A1 and A5 for exact definitions of $u(r)$ and $D^*(r)$. For reference, the diameter of a phospholipid molecule is approximately $\xi/2$ (if $\xi \simeq 15$ Å).

of large lipid domains can be expected to be small, the diffusion coefficients of integral proteins are not much smaller than those of lipids (Clegg & Vaz, 1985). Our treatment does not consider the problem of the mobility of the disks. However,

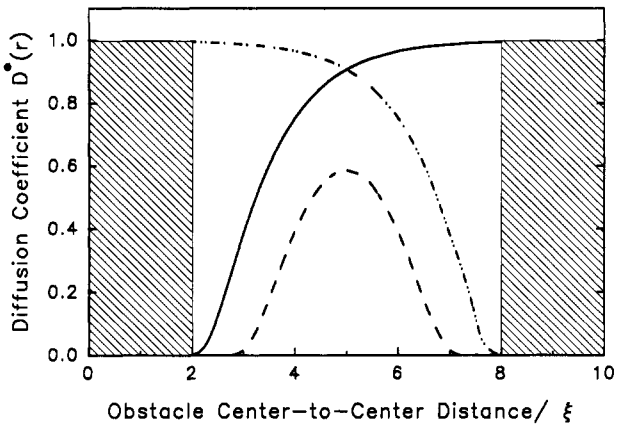

FIGURE 10: Effect of two neighboring obstacles on the diffusion coefficient $D^*(r)$ in the lipid fluid phase between them. The solid and dash–dot lines represent the effects of each obstacle per se, and the dashed line represents the cumulative effect of both obstacles. Other definitions are as in Figure 9.

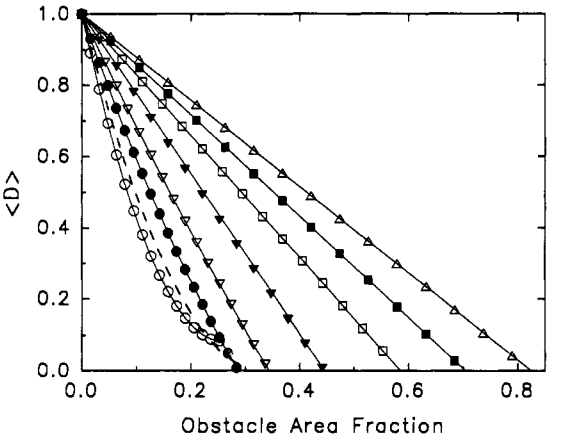

FIGURE 11: Dependence of the diffusion coefficient $\langle D \rangle$ on the obstacle area fraction for different obstacle radii. The points are calculated numerically from eq A11 and the lines are given by eq A12. The reduced radius R/ξ is 1.0 (○), 1.5 (●), 2.0 (▽), 3.0 (▼), 5.0 (□), 8.0 (■), and 15.0 (△). For values of R/ξ smaller than that corresponding to the dashed line (R/ξ = 1.17) the diffusion coefficient goes through a minimum before reaching zero (see text for a discussion of this aspect).

we expect eq A11 to be a good approximation for $\langle D \rangle$ in a system where boundary effects are important, when diffusion in the corresponding system where only hard core interactions occur is described by $\langle D \rangle = 1 - c$, for this is the limiting expression when $\delta \rightarrow 0$ (see Appendix). In which cases is $\langle D \rangle = 1 - c$ a useful approximation for the hard core repulsion problem? The parameters that must be considered are the radius of the obstacles (R) and the ratio γ of the mobility of a point tracer to the mobility of the obstacles. Monte Carlo simulations (Saxton, 1987) show that $\langle D \rangle = 1 - c$ is the correct expression for point obstacles when $\gamma \rightarrow 0$ (extremely mobile obstacles); it is also correct when $\gamma \rightarrow \infty$ (immobile obstacles) and R is sufficiently large [see Figure 5 of Saxton (1989)]—in practice, this means $R > 10d$, approximately, where d is the lattice constant. If these units are translated into real dimensions, the tracer being a fluid lipid, this corresponds approximately to $R > 80$ Å, which is the size of the solid obstacles determined for LigGalCer/DPPC, 20:80.

For obstacles of intermediate size, $\langle D \rangle = 1 - c$ if the mobility of the obstacles is also intermediate. This conclusion is based on Monte Carlo simulations of the dependence of the diffusion coefficient on the size of mobile hexagonal obstacles (Saxton, 1988). If $R = 3d$, we find from those results that $\langle D \rangle = 1$

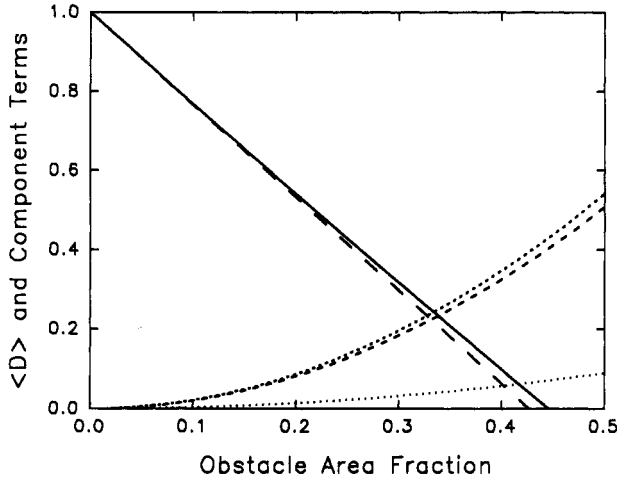

FIGURE 12: Relative diffusion coefficient $\langle D \rangle$ (solid line) and its component terms, calculated for $R/\xi = 3.0$. The long dashed line is eq A10. The other lines are the correction terms in eq A11. The medium dashed curve is the integral of the overlap area (second term inside the first bracketed term in eq A11). The short dashed curve is the integral of $D^*(r)$ over the overlap area (second term inside the second bracketed term in eq A11). The dotted line (smallest term) is the integral of the modified $D^*_{overlap}(r)$ over the overlap regions.

$-c$ if $\gamma \simeq 1.3$. The diffusion coefficient is not very sensitive to small changes in γ; to give an idea of the effect, if $\gamma \simeq 1.8$ and $R = 3d$, then $\langle D \rangle \simeq (1 - c)/1.05$. The case of $R = 3d$ is interesting because it corresponds to protein obstacles with $R \simeq 24$ Å, which is the size of most proteins used by Blackwell and Whitmarsh (1990). Assuming that it is correct to identify γ of a Monte Carlo simulation with the ratio of the diffusion coefficients of lipid to protein, we have $\gamma \simeq 1.8$, corresponding to a protein of this size with $D \simeq 3.3 \times 10^{-8}$ cm^2/s (Clegg & Vaz, 1985), and a lipid with $D \simeq 6 \times 10^{-8}$ cm^2/s (Vaz et al., 1985b), at about 35 °C. This is clearly in the range where only about 5% error will result from using $\langle D \rangle = 1 - c$ for the hard core problem. The same equation works reasonably well both for large, immobile lipid solid-phase obstacles and for mobile, integral protein obstacles because the diffusion coefficient of the obstacle decreases as the radius increases (though not necessarily linearly).

In the model now proposed, several approximations were made in the derivation of the final expression (eq A11). Moreover, the assumption of obstacles with a constant radius was also made, which may be incorrect in the case of lipid solid-phase domains. Unfortunately, the lack of precise knowledge of ξ diminishes the prediction capabilities of the model, which renders it more difficult to disprove. On the other hand, the calculated curves for the diffusion coefficient as a function of obstacle area are very sensitive to size (for small and medium sizes) once a value is chosen for ξ (Figure 11). And if the idea of the existence of a boundary layer as described is correct, it is not reasonable to expect ξ to have values much outside the 10–20-Å range. An independent measurement of domain size could be used to determine ξ. In the case of the integral membrane proteins studied by Blackwell and Whitmarsh (1990), the calculations lead to $\xi \simeq 22$ Å for all proteins. The work presented here is a tentative resolution of the long-standing conflict between theory and experiment on the problem of diffusion in an archipelago (Saxton, 1987). However, it is clear that the model developed gives only an approximate solution for the problem. Improvement in the theoretical derivation is certainly possible.

Percolation in the LigGalCer/DPPC System. The existence of a percolation point requires that the clusters constituting the two phases be immobile (Harrison & Zwanzig, 1985; Saxton, 1987, 1990). Experimentally, the possibility of determining such a point in a lipid mixture requires that the time scale of the mobility and the lifetime of the solid-phase domains be very large compared to lipid diffusion. The dynamic aspects of the solid clusters will shift the apparent percolation point—as determined by a FRAP experiment—to a higher fraction of solid, leading to uncertainty in its identification. Our interpretation lies therefore upon the assumption of essentially immobile and long-lived solid domains; whereas this was not a critical aspect in the interpretation of the behavior of the diffusion coefficient, it is important to realize that it becomes absolutely essential here, at least *at the percolation threshold.* In the case of the mixture LigGalCer/DPPC, 20:80, the available information argues in favor of the correctness of our interpretation. The high nonideality of mixing of the two components, as revealed by calorimetry, results in the formation of phases of very different composition. This in turn presumably leads to longer lifetimes for the domains because the molecules that constitute a solid domain have to diffuse physically to a certain extent out of a given region before this region can become fluid. Moreover, at the percolation threshold, an abrupt increase in τ ($\tau \rightarrow \infty$, $D \rightarrow 0$) is the behavior expected (Stauffer, 1985; Saxton, 1982, 1987), and this is exactly what is observed experimentally.

It became apparent to us, in the course of a discussion with Dr. Rodney Biltonen, that the increase in the dispersion around the mean values of the percent recovery and the recovery time observed in the region of the percolation threshold (Figures 3, 4, and 6) may have a precise significance. The very small variances observed outside the percolation region indicate that the dispersion in this region is not an experimental problem but a property of the system. These large standard deviations probably arise because, in the multibilayer stack, each bilayer exists in one of two states: either above or below the percolation threshold. Note that both states would have the same fraction of solid phase, but different geometric configurations of this phase lead to different percolation states. Bilayers above the threshold contribute 1 to the ensemble percolation probability, and bilayers below the threshold contribute zero; there are essentially no bilayers contributing, say, 0.5. Alternatively, the variances could result from thermal fluctuations, which would in turn lead to fluctuations in the solid area. Using the curve shown in Figure 6 and the uncertainty in the temperature control, we have calculated the expected variances for this case; they are systematically lower than those experimentally observed, though more experiments are necessary to firmly establish this fact.

Solid-Domain Topology across the Lipid Bilayer. The comparative study of diffusion using NBD-msPE and NBD-POPE (or NBD-DLPE) indicates that the arrangement of the solid domains across the bilayer in binary lipid mixtures is not the same in all mixtures. In DMPC/DSPC the solid domains are exactly superimposed upon each other in the two monolayers whereas in LigGalCer/DPPC they are not.

In LigGalCer/DPPC, 20:80, the apparent percolation point determined with NBD-msPE—identified by the abrupt increase in τ—occurs at a lower solid fraction (higher temperature) than the percolation point in each monolayer (determined by NBD-POPE). This clearly indicates that solid domains are not superimposed across the lipid bilayer. In the solid/fluid coexistence region, the transmembrane probe simultaneously senses the distribution of solid domains in the two leaflets of the bilayer. If the solid domains in the two apposing monolayers were exactly superimposed upon each

other, the diffusion of the two probes would be the same, once corrected for the intrinsic difference in the magnitude of the values of τ in the fluid phase. However, if the positions of the solid domains in one monolayer are not correlated with their positions in the other monolayer, the effective number of domains sensed by the transmembrane probe is greater and the apparent percolation point occurs at a lower fraction of solid. At this point, the system has reached a configuration where a snapshot would reveal the existence of a percolating cluster of solid obstacles if we count domains in both monolayers. Moreover, at temperatures above the percolation threshold, the values of the diffusion coefficient of NBD-msPE fall exactly on the curve describing the dependence of the diffusion constant on the solid fraction for NBD-POPE (Figure 7), if we assume that the position of the solid domains in the two apposing monolayers is completely random. In plotting the points corresponding to NBD-msPE on the curve, the solid area assigned to each value of the diffusion coefficient is the effective solid area fraction (c_{eff}) felt by the transmembrane probe. This area fraction is given by $c_{eff} = 1 - p^2$, where p is the actual fluid area fraction in each monolayer. This expression results simply from a binomial expansion: p^2 is the probability of having fluid superimposed onto fluid phase in the other monolayer, if the relative positions of the domains are random. The corresponding curve for τ as a function of temperature was calculated and plotted in Figure 4.

In DMPC/DSPC, 50:50, at equilibrium, the curves of τ and percent recovery as a function of temperature are the same with NBD-msPE and NBD-DLPE, indicating that the solid domains are exactly superimposed upon each other across the lipid bilayer. A considerable hysteresis was observed in the cooling and heating curves when NBD-msPE was the probe used but not when NBD-DLPE was employed. One possible explanation for this behavior is that, in the heating scan, a state close to equilibrium is reached independently in each monolayer, but the system is still away from the global bilayer equilibrium. Two incoherent networks of solid domains could thus exist in each monolayer, and the relaxation to the more stable state where the solid phases are exactly superimposed would be extremely slow (half-time greater than 7 h). This interpretation, however, is probably inconsistent with the lack of hysteresis in calorimetry (R. L. Biltonen, personal communication), unless the transbilayer coupling of the domains would have a very small enthalpy associated with it. An alternative possibility is that, after prolonged incubation in the all-solid phase, the transmembrane probe gets trapped into solid domains, where it is essentially completely immobile. The smaller recovery observed in the heating scans would in this case be the result of bleaching of solid-phase areas containing the probe which would not recover. The values of τ are not significantly different in the cooling and heating scans, which argues in favor of this interpretation: the probes that do diffuse do so in the same fashion in both scaning modes.

It is not completely clear to us why there is a difference in the transbilayer solid-phase topology in the these two mixtures. One possible reason is that the solid phase in DMPC/DSPC, 50:50, seems to be a $P_{\beta'}$ phase, by freeze–etch electron microscopy (Rock et al., 1991), which must, by definition, be superimposed onto itself across the lipid bilayer.

The transbilayer organization of domains may have significant consequences for biological membranes. The lipid composition of the inner and outer monolayers is very different in most cell plasma membranes (Rouser et al., 1968; Op den Kamp, 1979; Cullis & Hope, 1985). As a result, the structures and the amounts of the solid phases which may occur at a given temperature are also likely to be different. On this basis, it is expected that the phases in the apposing monolayers will not necessarily be correlated. In addition, most membrane proteins span the lipid bilayer. In any physiological process requiring diffusion of these integral proteins, the obstructing effect of solid domains (from which they are generally excluded) will be very much enhanced if the phases are not correlated across the bilayer. This effect may manifest itself dynamically, in a reduction of the mobility of integral membrane proteins, or structurally, leading to compartmentalization of these proteins in different pools, which will have important consequences for reactions occurring in the plane of the membrane (Thompson et al., 1992).

ACKNOWLEDGMENT

We thank Dr. Thomas Jovin for his support of this work, Dr. Rodney Biltonen and Dr. Gordon Rule for useful discussions, and Dr. M. B. Sankaram for his critical reading of the manuscript. The FRAP curve-fitting and analysis programs were kindly provided by Dr. Eurico Melo. We also acknowledge Dr. Biltonen and Kim Thompson's cooperation in the calorimetry. Finally, we thank especially Stéphane Clerc for his invaluable help with the numerical evaluation of eq A11 and Dr. Michael Saxton for extremely helpful criticism and suggestions.

APPENDIX

In this section, we derive an expression for the diffusion coefficient of a fluid-phase lipid molecule (hereafter also called a tracer) in a lipid bilayer in the presence of impermeable obstacles for diffusion. These obstacles can be solid-phase domains, where the tracer molecule is insoluble, or integral membrane proteins. The obstacles reduce the diffusion coefficient of a tracer (a) by hard core repulsion, preventing movement across them, and (b) by increasing the order of the fluid-phase lipids in their neighborhood. First, we consider the effect of one obstacle on the annulus of adjacent fluid phase. Second, we evaluate the diffusion coefficient of a tracer in a system containing a large number of these obstacles.

Diffusion Coefficient in the Neighborhood of a Solid-Phase Obstacle. The problem of the influence of an integral membrane protein on the orientational order parameter of adjacent lipid molecules has been the subject of experimental (Vaz et al., 1978; Marsh & Watts, 1982) and theoretical research (Marčelja, 1976; Owicki et al., 1978; Owicki & McConnell, 1979; Jähnig, 1981; Sperotto & Mouritsen, 1991) [see also, Abney and Owicki (1985) and references cited therein]. The behavior of the lipid order parameter away from an obstacle is found to be well described by a simple exponential decay function (Owicki et al., 1978). Here we treat a solid domain in the same fashion as a protein molecule or, more generally, simple as a cylindrical impermeable obstacle embedded in the membrane. The relative free area per lipid molecule can be written in terms of the function (see Figure 9) describing the change in the order parameter away from the obstacle

$$u(r) = 0 \qquad r < R$$

$$u(r) = 1 - (1 - u_o) \exp[-(r - R)/\xi] \qquad r \geq R \qquad \text{(A1)}$$

where $u(r) = a_f(r)/a_{f_o}$ is the relative free area, defined as the ratio of the free area at a distance $r - R$ from the obstacle boundary [$a_f(r)$] to the free area in the bulk fluid phase (a_{f_o}).

Note that according to this definition, $u = 0$ corresponds to order and $u = 1$ corresponds to disorder. The origin of the radial distance r is chosen at the center of the obstacle of radius R. At the boundary, the relative free area has the value u_o. This parameter reflects the interactions of the fluid-phase molecule with the obstacle. Its magnitude is discussed by Jähnig (1981). For the case treated here, it should have a value between 0.0 and 0.5. We keep it constant with an intermediate value of 0.25, but this particular choice has little influence on the calculations. The obstacle influence decays with a coherence length ξ of approximately 15 Å [Jähnig (1981); see also comparison with the results of Marsh and Watts (1982) below]. We would expect it to vary between 10 and 20 Å, depending on the system. Strictly speaking, ξ must also be a function of the absolute temperature (T); a priori, ξ is expected to vary as $1/T$. However, for short temperature intervals (of the order of 10 °C), this variation is very small, so that most of the error in the estimation of ξ arises from the initial value chosen. Therefore, we treat ξ as a constant in this work. The only true variable parameter in the model is the reduced radius R/ξ. For convenience and generality, we use ξ as the unit of length in all theoretical calculations.

According to the free-area model for lipid diffusion (Galla et al., 1979; McCarthy & Kozak, 1982; Vaz et al., 1985b; Clegg & Vaz, 1985) based on the free-volume theory for diffusion in liquids and glasses (Cohen & Turnbull, 1959), the diffusion coefficient D depends exponentially on the free area. We use the modification for a two-dimensional system derived by McCarthy and Kozak (1982). In a homogeneous system, the diffusion coefficient is defined as an integral over the distribution of free area

$$D = \int_{a_s}^{\infty} D(a)p(a)\,da \qquad \text{(A2)}$$

where $D(a)$ is the diffusion constant inside a free area a, $p(a)$ is the probability of finding a free area of size a, and a_s is the critical free area; areas below a_s are useless for diffusion. In a two-dimensional system a_s is the closed-packed area for disks; in a lipid system this is simply the molecular area in the solid phase.

The probability density $p(a)$ is given by

$$p(a) = 1/a_f \exp(-a/a_f) \qquad \text{(A3)}$$

where a_f is the average free area in the system, related to the total area/particle a_t by $a_f = a_t - a_s$. Following Cohen and Turnbull (1959), $D(a)$ is assumed constant and the expression for the diffusion coefficient becomes

$$D = D(a) \exp(-a_s/a_f) \qquad \text{(A4)}$$

In a two-phase system, we define a normalized diffusion coefficient D^* as the ratio of the diffusion coefficient at a given region to its value in the bulk fluid phase D_o

$$D^*(r) = \frac{D}{D_o} = \exp\left[\left(\frac{a_s}{a_{f_o}}\right)\left(1 - \frac{1}{u(r)}\right)\right] \qquad \text{(A5)}$$

where a_{f_o} is the free area in the bulk fluid phase. The ratio a_s/a_{f_o} has a value of approximately 2.5 for saturated diacylphosphatidylcholines, corresponding to an area of about 63 Å^2 for the fluid phase and 45 Å^2 for the lipid solid phase (Almeida et al., 1992; Lewis & Engelman, 1983; Wiener et al., 1989). It is weakly temperature dependent except very close to the main phase transition. We assume it to be constant in the present analysis.

The functions representing the relative diffusion coefficient and the relative free area in the neighborhood of an obstacle are represented in Figure 9 in units of the coherence length (ξ). The resulting curve for D^* is in very good agreement with the results of Marsh and Watts (1982), which indicate that the first lipid molecule next to a protein is virtually immobilized, but the approach to the bulk value of the mobility is very rapid in the subsequent lipid layers.

Diffusion Coefficient in a Lipid Bilayer in which Solid and Fluid Phases Coexist. We derive now an expression for the diffusion coefficient in a two-phase system. Strictly, the theory is applicable only to systems with more than one component, because fluctuations in a pure lipid system at the phase transition invalidate the assumptions of our model. The applicability of the model should be better the greater the nonideality of the mixture because of the concomitant decrease in fluctuations. The average relative diffusion coefficient $\langle D \rangle$ is defined as the ratio of the diffusion coefficient measured in the composite medium to the diffusion coefficient that would be observed if the same system were entirely in the fluid state (no obstacles present). We treat the composite medium as a two-dimensional system composed of nonoverlapping solid-phase obstacles randomly distributed in a homogeneous matrix of fluid phase. The solid obstacles are modeled as impenetrable disks of uniform radius R, plus an annular region, determined by the coherence length ξ, which extends appreciably into the fluid phase within a length δ (Figure 9). The annular regions can overlap to any extent including overlap with the core regions. The lifetime of solid-phase obstacles is assumed to be much longer than the characteristic time of lipid diffusion. As a simple result of a random distribution, the disks may "aggregate" to form the actual solid domains, the size of which will increase with increasing obstacle density. An alternative way of interpreting the model is as if the solid-phase regions were obtained by juxtaposition of disks of an appropriate size.

Consider thus a two-dimensional system S of radius $R_S \gg R$. In the absence of obstacles the relative diffusion coefficient $\langle D \rangle$ equals 1 by definition. We now place, at the origin of the system S, a disk of radius R and annulus of influence δ. The relative diffusion coefficient is still defined by an expression analogous to the case of a homogeneous system:

$$\langle D \rangle = \frac{\int_{\text{two-phase}} 2\pi r\,dr\rho(r) \int_{a_s}^{\infty} D(a)p(a,r)\,da}{\int_{\text{fluid}} D(a)p(a)\,da} \qquad \text{(A6)}$$

In the two-phase system, $p(a,r)$ becomes a function of the position of the disks. The probability density $p(a,r)$ is formally identical to $p(a)$ but now a_f depends on r: $a_f(r) = a_{f_o}u(r)$, where $u(r)$ is given by eq A1. The disk density $\rho = N/\pi R_S^2$, where N is the number of disks. For the moment we are considering the case $N = 1$, so $\rho = 1/\pi R_S^2$. In eq A6, $D(a)$ is a constant and drops out; the denominator is simply our result for the fluid phase, $\exp(-a_s/a_{f_o})$.

Now we integrate first over the free area. Using eqs A1 and A5, we obtain, after some simple manipulations

$$\langle D \rangle = \int_{\text{two-phase}} 2\pi\rho(r)D^*(r)r\,dr \qquad \text{(A7)}$$

where $D^*(r)$ is given by eq A5. The diffusion coefficient $\langle D \rangle$ becomes simply an average of $D^*(r)$ over the different regions of the system. This integral has to be broken up into three regions: inside the disk $0 < r < R$, within the annulus $R <$

$r < R + \delta$, and in the bulk fluid $r > R + \delta$

$$\langle D \rangle = \left[\int_0^R 2\pi D^*(r) r \, dr + \int_R^{R+\delta} 2\pi D^*(r) r \, dr + \int_{R+\delta}^{R_S} 2\pi D^*(r) r \, dr \right] / \pi R_S^2 \quad \text{(A8)}$$

where the explicit form of ρ has been used. The first integral in eq A8 is zero because $D^*(r) = 0$ for $0 < r < 1$; this arises because $a = a_S$ inside the solid. The second integral corresponds to the annular region. The third integral corresponds to the bulk fluid phase and can be evaluated because $D^*(r) = 1$ for $r > R + \delta$. Thus, for a system with one disk

$$\langle D \rangle = 1 - \frac{\pi(R+\delta)^2}{\pi R_S^2} + \frac{\int_R^{R+\delta} 2\pi D^*(r) r \, dr}{\pi R_S^2} \quad \text{(A9)}$$

When a small enough number N of circles is present, there is no overlap between their annuli and the expression for the diffusion coefficient is a simple extension of eq A9; multiplying the second and third terms by N yields

$$\langle D \rangle = 1 - \rho\pi(R+\delta)^2 + \rho \int_R^{R+\delta} 2\pi D^*(r) r \, dr \quad \text{(A10)}$$

Notice that the density ρ is related to the obstacle area fraction c by $\rho = c/\pi R^2$.

When more disks are added to the plane (in a random way, except that overlap of the hard cores is forbidden), some of their annular regions begin to overlap. At high disk densities multiple overlaps occur. We will ignore overlaps higher than pairs. However, at moderate obstacle densities, a correction for overlap of pairs of obstacle annuli can be obtained by adding three extra terms to $\langle D \rangle$ in eq A10. Consider again a circle with its center at the origin and let $P(s)$ be the probability that another circle is centered at point B, at a distance s from the origin. When $s < 2(R + \delta)$, the annuli will overlap in an area delimited by the outer radii of the annuli of the two circles. This area is the sum of two segments of circle (see, for example, *CRC Standard Mathematical Tables*), defined by the outer radius $R + \delta$, and half the center-to-center distance $s/2$. This distance determines the angle $\alpha = \cos^{-1} s/[2(R + \delta)]$ defined by the lines $\overline{OB}$ and $\overline{OI}$, where I is the point of intersection of the outer radii $R + \delta$ of the annuli of the two obstacles. To calculate the area, integration is performed over the polar coordinates r and θ; r varies between $r_1 = s \cos\theta - [(R + \delta)^2 - s^2 \sin^2\theta]^{1/2}$ and $r_2 = R + \delta$, and θ varies between $-\alpha$ and α. Equation A10 is thus modified to take into account annuli overlap in the following way. The second term in (A11) is corrected by subtracting from it, the overlap area. The third term in (A11) is corrected by subtracting from it the integral of $D^*(r)$ over the overlap area. Finally, diffusion in the overlap area is added as the integral of a $D^*_{\text{overlap}}(r)$, which will be defined below. We then obtain

$$\langle D \rangle = 1 - \rho\left[\pi(R+\delta)^2 - \frac{1}{2}\int_{2R}^{2(R+\delta)} P(s) \int_{-\alpha}^{\alpha}\int_{r_1}^{r_2} r \, dr \, d\theta \, ds \right] + \rho\left[\int_R^{R+\delta} 2\pi D^*(r) r \, dr - \int_{2R}^{2(R+\delta)} P(s) \int_{-\alpha}^{\alpha}\int_{r_1}^{r_2} D^*(r) r \, dr \, d\theta \, ds \right] + \rho\left[\frac{1}{2}\int_{2R}^{2(R+\delta)} P(s) \int_{-\alpha}^{\alpha}\int_{r_1}^{r_2} D^*_{\text{overlap}}(r) r \, dr \, d\theta \, ds \right] \quad \text{(A11)}$$

The limits of integration over s prevent overlap of the hard cores. The factors of $^1/_2$ in the correction term for the area and in the integral of $D^*_{\text{overlap}}(r)$ appear because the correction per obstacle is only half the correction per pair. However, in the correction term corresponding to $D^*(r)$ this factor is not included, because correction is necessary for each obstacle annulus in each pair.

In the overlapping annular areas, the relative diffusion coefficient $D^*_{\text{overlap}}(r)$ is subject to the simultaneous influence of two neighboring obstacles. The form of $D^*_{\text{overlap}}(r)$ can only be given approximately. We define the free area in the overlap regions by $u_{\text{overlap}} = u(r)u(s-r)$ and obtain the diffusion coefficient from eq A5. This form is similar to Schröder's equation (Abney & Owicki, 1985). In the regions of simultaneous influence of two obstacles the diffusion coefficient decreases quite dramatically, as shown in Figure 10 for $s/\xi = 10$ and $R/\xi = 2$.

The probability function $P(s)$ depends on the pair correlation function in two dimensions, which is not known exactly in analytical form (Berryman, 1983). This prevents an exact analytical evaluation of the integrals in eq A11. We use here the simplest approximation, $P(s) = 2\pi\rho s$. Even this approximation, we were unable to perform the integration in the last two correction terms analytically. Therefore, we evaluated $\langle D \rangle$ as a function of the obstacle area fraction c from eq A11 numerically. The calculation was repeated for several different values of R/ξ and the numerical data were fitted to a second-order polynomial in the obstacle area fraction c, where the coefficients a and b are functions of the reduced radius R/ξ (no physical significance is attached to the numerical parameters in these functions).

$$\langle D \rangle = 1 + ac + bc^2$$

$$a = -1.208 - 24.3 \exp(-1.763R/\xi) - 2.408 \exp(-0.3138R/\xi) \quad \text{(A12)}$$

$$b = 185 \exp(-2.587R/\xi)$$

The dependence of the relative diffusion coefficient on the obstacle area fraction is shown in Figure 11 for different values of R/ξ. If $R/\xi < 1.17$ the curve of $\langle D \rangle$ reaches a minimum before going through zero. This minimum makes no physical sense and simply means that the approximations used break down for values of c greater than that corresponding to the minimum. As R/ξ gets smaller for a given c, the annuli become a comparatively higher fraction of the system. The overlapping areas thus increase and the error in the approximations becomes larger. It would then be necessary to take into account overlap between triplets of obstacle annuli which the model ignores. For $R/\xi > 3$ the coefficient b in eq A12 can be set to zero, the linear equation $\langle D \rangle = 1 + ac$ being an excellent approximation for all purposes. The numerical expression should be used only for R/ξ smaller than about 20. An expression extending to higher values could be given but would have to contain more numerical parameters. However, for large radii, the diffusion coefficient becomes insensitive to obstacle size, and the interest of a more general formula is rather limited. The reason for the linearity if $R/\xi > 3$ can be understood with reference to Figure 12, where the different terms contributing to $\langle D \rangle$ are shown as functions of c. The integrals correcting for the annular overlap areas and for the diffusion coefficient $D^*(r)$ in these areas have opposite signs and similar magnitudes and therefore almost cancel out. The value of the modified $D^*_{\text{overlap}}(r)$ is very small for most of the

range of c. We must keep in mind, however, that these results are obtained with an approximate form for $P(s)$ and may not apply in general if the exact form were used instead.

It is known that obstacle mobility affects the diffusion of a tracer in Monte Carlo simulations (Saxton, 1987). So far, nothing has been said about the mobility of the obstacles in our model; it does not enter the derivation. However, it is possible to assess the range of applicability of our result by making $\delta \rightarrow 0$ in eq A11, which yields the corresponding expression for a system where only had core repulsions exist (such as those simulated by Saxton). Taking the limit $\delta \rightarrow 0$, one obtains simply $\langle D \rangle = 1 - c$. Thus, eq A11 should approximate the solution of the problem involving annular regions as $\langle D \rangle$ $1 - c$ approximates the solution for the hard core interaction problem, in an otherwise identical system. According to Xia and Thorpe (1988), if the obstacles are embedded in a continuum, we have $\langle D \rangle = 1 - 2c$, independently of obstacle size. In contrast, lattice Monte Carlo simulations indicate that the diffusion coefficient depends on the obstacle size (Saxton, 1989) and that, for mobile obstacles, $\langle D \rangle = 1 - c$ is closer to the correct c-dependence of $\langle D \rangle$ than is $\langle D \rangle = 1 - 2c$.

REFERENCES

Abney, J. R., & Owicki, J. C. (1985) In *Progress in Protein–Lipid Interactions* (Watts, A., & De Pont, J. J. H. H. M., Eds.) Vol. 1, pp 1–60, Elsevier, Amsterdam.

Almeida, P. F. F., Vaz, W. L. C., & Thompson, T. E. (1992) *Biochemistry* (in press).

Bartlett, G. R. (1959) *J. Biol. Chem. 234*, 466–468.

Berryman, J. G. (1983) *Phys. Rev. A. 27*, 1053–1061.

Blackwell, M. F., & Whitmarsh, J. (1990) *Biophys. J. 58*, 1259–1271.

Bultmann, T., Vaz, W. L. C., Melo, E. C. C., Sisk, R. B., & Thompson, T. E. (1991) *Biochemistry 30*, 5573–5579.

Clegg, R. M., & Vaz, W. L. C. (1985) In *Progress in Protein–Lipid Interactions* (Watts, A., & De Pont, J. J. H. H. M., Eds.) Vol. 1, pp 173–229, Elsevier, Amsterdam.

Cohen, M. H., & Turnbull, D. (1959) *J. Chem. Phys. 31*, 1164–1169.

CRC Standard Mathematical Tables (1990) p 125, CRC Press, Boca Raton, FL.

Cullus, P. R., & Hope, M. J. (1985) In *Biochemistry of Lipids and Membranes* (Vance, D. E., & Vance, J. E., Eds.) Chapter 2, pp 28–33, Benjamin/Cummings, Menlo Park, CA.

Einstein, A. (1926) *Investigations on the Theory of the Brownian Movement* (Fürth, R., Ed.) pp 36–67, Dover, New York.

Galla, H.-J., Hartmann, W., Theilen, U., & Sackmann, E. (1979) *J. Membr. Biol. 48*, 215–236.

Harrison, A. K., & Zwanzig, R. (1985) *Phys. Rev. A 32*, 1072–1075.

Jähnig, F. (1981) *Biophys. J. 36*, 329–345.

Lewis, B. A., & Engelman, D. M. (1983) *J. Mol. Biol. 166*, 211–217.

Mabrey, S., & Sturtevant, J. M. (1976) *Proc. Natl. Acad. Sci. U.S.A. 73*, 3862–3866.

MacCarthy, J. E., & Kozak, J. J. (1982) *J. Chem. Phys. 77*, 2214–2216.

Macedo, P. B., & Litovitz, T. A. (1964) *J. Chem. Phys. 42*, 245–256.

Marsh, D., & Watts, A. (1982) In *Protein–Lipid Interactions* (Jost, P. C., & Griffith, O. H., Eds.) Vol. 2, pp 53–126, Wiley, New York.

Maggio, B., Ariga, T., Sturtevant, J. M., & Yu, R. K. (1985a) *Biochim. Biophys. Acta 818*, 1–12.

Maggio, B., Ariga, T., Sturtevant, J. M., & Yu, R. K. (1985b) *Biochemistry 24*, 1084–1092.

Marčelja, S. (1976) *Biochim. Biophys. Acta 455*, 1–7.

Nagle, J. F., & Wilkinson, D. A. (1978) *Biophys. J. 23*, 159–175.

O'Leary, T. J. (1987) *Proc. Natl. Acad. Sci. U.S.A. 84*, 429–433.

Op den Kamp, J. A. F. (1979) *Annu. Rev. Biochem. 48*, 47–71.

Owicki, J. C., & McConnell, H. M. (1979) *Proc. Natl. Acad. Sci. U.S.A. 76*, 4750–4754.

Owicki, J. C., Springgate, M. W., & McConnell, H. M. (1978) *Proc. Natl. Acad. Sci. U.S.A. 75*, 1616–1619.

Pink, D. A., Geogallas, A., & Chapman, D. (1981) *Biochemistry 20*, 7152–7157.

Rock, P., Allietta, M., Young, W. W., Thompson, T. E., & Tillack, T. W. (1991) *Biochemistry 30*, 19–25.

Rouser, G., Nelson, G. J., Fleischer, S., & Simon, G. (1968) In *Biological Membranes, Physical Fact and Function* (Chapman, D., Ed.) Chapter 2, Academic Press, London and New York.

Sankaram, M. B., & Thompson, T. E. (1990) *Biochemistry 29*, 10676–10684.

Saxton, M. J. (1982) *Biophys. J. 39*, 165–173.

Saxton, M. J. (1987) *Biophys. J. 52*, 989–997.

Saxton, M. J. (1988) *Biophys. J. 53*, 510a.

Saxton, M. J. (1989) *Biophys. J. 56*, 615–622.

Saxton, M. J. (1990) *Biophys. J. 57*, 1167–1177.

Soumpasis, D. M. (1983) *Biophys. J. 41*, 95–97.

Shimshick, E. J., & McConnell, H. M. (1973) *Biochemistry 12*, 2351–2360.

Sperotto, M. M., & Mouritsen, O. G. (1991) *Biophys. J. 59*, 261–270.

Stauffer, D. (1985) *Introduction to Percolation Theory*, Taylor & Francis, London and Philadelphia.

Suurkuusk, J., Lentz, B. R., Biltonen, R. L., & Thompson, T. E. (1976) *Biochemistry 15*, 1393–1401.

Thompson, T. E., Sankaram, M. B., & Biltonen, R. L. (1992) *Comments Mol. Cell. Biophys. 8*, 1–15.

Vaz, W. L. C., & Hallmann, D., (1983) *FEBS Lett. 152*, 287–290.

Vaz, W. L. C., Vogel, H., Jähnig, F., Austin, R. H., & Schoellmann, G. (1978) *FEBS Lett. 87*, 269–272.

Vaz, W. L. C., Hallmann, D., Clegg, R. M., Gambacorta, A., & De Rosa, M. (1985a) *Eur. Biophys. J. 12*, 19–24.

Vaz, W. L. C., Clegg, R. M., & Hallmann, D. (1985b) *Biochemistry 24*, 781–786.

Vaz, W. L. C., Melo, E. C. C., & Thompson, T. E. (1989) *Biophys. J. 56*, 869–876.

Vaz, W. L. C., Melo, E. C. C., & Thompson, T. E. (1990) *Biophys. J. 58*, 273–275.

Wiener, M. C., Suter, R. M., & Nagle, J. F. (1989) *Biophys. J. 55*, 315–325.

Wu, S. H., & McConnell, H. M. (1975) *Biochemistry 14*, 847–854.

Xia, W., & Thorpe, M. F. (1988) *Phys. Rev. A 38*, 2650–2656.

Registry No. DMPC, 18194-24-6; DPPC, 63-89-8; DSPC, 816-94-4; LigGalCer, 142260-93-3; NBD-DLPE, 142260-94-4; POPE, 26662-94-2.